PUBLICATIONS OF THE EARTH PHYSICS BRANCH

VOLUME 40–NO. 1

a ferrite core fluxgate magnetometer

F. PRIMDAHL

DEPARTMENT OF ENERGY, MINES AND RESOURCES
OTTAWA, CANADA 1970

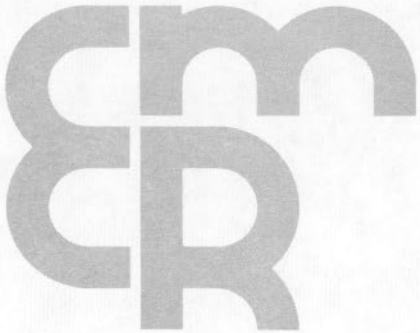

PUBLICATIONS OF THE EARTH PHYSICS BRANCH

VOLUME 40–NO. 1

a ferrite core fluxgate magnetometer

F. PRIMDAHL

DEPARTMENT OF ENERGY, MINES AND RESOURCES
OTTAWA, CANADA 1970

Cat. No.: M70-40/1

Contents

a ferrite core fluxgate magnetometer

F. PRIMDAHL

Abstract. A fluxgate magnetometer was designed and constructed to investigate the possibility of achieving the long-term stability required of the primary recording instruments at a standard magnetic observatory. An orthogonally-gated sensor is used, with a tubular ferrite core. The instrument was set up to measure total intensity, and compared with a proton precession magnetometer. The first test showed a drift of 2.5 gammas in 15 days. A second stability test gave an initial drift of 9 gammas over the first 20 days followed by random fluctuations of ±3.5 gammas over the next 60 days.

Résumé. Dans la présente étude, l'auteur décrit la conception, le montage et les essais d'un magnétomètre à noyau saturé construit afin d'étudier la possibilité d'obtenir la stabilité à long terme exigée des appareils enregistreurs primaires utilisés dans les observatoires magnétiques de type courant. L'appareil expérimental comprend un élément sensible à un noyau de ferrite tubulaire orthogonallement excité. L'instrument, réglé pour mesurer l'intensité totale, a été comparé à un magnétomètre à protons. Le premier essai a indiqué une déviation de 2.5 gammas en 15 jours; dans un deuxième essai de stabilité, un glissement initial de 9 gammas s'est produit au cours des vingt premiers jours, puis des fluctuations irrégulières de ± 3.5 gammas dans les 60 jours suivants.

Introduction

The equipment used at most magnetic observatories for recording the natural variations of the geomagnetic field has not changed in principle for over a century. The angular deflections of delicately suspended magnets are optically magnified and recorded on slowly moving photographic paper. Magnetometers producing an electrical signal proportional to the magnetic variations have several advantages over the classical instruments. The signal can be recorded at a distance from the sensor, requiring less elaborate nonmagnetic buildings, and the record is immediately visible. Of growing importance is the ease with which electrical signals can be recorded in digital form, to take advantage of computer methods of analysis and data storage. However, magnetic observatories have been slow to adopt electrical magnetometers, partly because of the cost, but chiefly because the new systems have not equalled a first-class set of photographic instruments in reliability and long-term stability.

Of the various types of electrical magnetometers which might prove suitable for recording the geomagnetic elements at a standard magnetic observatory, the fluxgate instrument is probably the simplest and least expensive. Recording fluxgate magnetometers are widely used at temporary magnetic observatories and as low-sensitivity instruments at permanent observatories, but they have generally been considered not quite good enough for primary equipment at a standard observatory because of unexplained temperature effects and occasional sudden shifts in output level.

This paper describes the design, construction and testing of a fluxgate magnetometer intended to maintain a stability of the order of 1 gamma over a period of several weeks. An orthogonally-gated sensor with a tubular ferrite core was chosen for the investigation. The electronic circuit was carefully designed to eliminate as far as possible sources of drift and offset in this part of the instrument, and to permit the evaluation of each component of the magnetometer.

The theory of the orthogonally-gated fluxgate has been reviewed by Primdahl (in press).

The sensor

The sensor is of the form described by Alldredge (1958) and Ling (1963, 1965). It consists of a Permax 35 ferrite tube, outside diameter 4 mm, inside diameter 2 mm and length 120 mm, manufactured by Ferroperm, Naerum, Denmark. The excitation winding is wound toroidally through the tube in the way suggested by Ling to eliminate the resultant pitch about the tube axis. The ferrite tube and excitation winding are potted inside a 150 mm long quartz tube, which also serves as coil former for the secondary winding. As Joukova (1949) predicted and showed experimentally, the core is very sensitive to torsion, so that a slight twisting of the ends of the tube couples a large amount of the excitation flux to the secondary coil. Axial pressure applied to the ends produces no noticeable effect.

A number of excitation and secondary windings have been tried: 10 to 30 turns for the excitation depending on the available current and voltage, and 500 to 3000 turns for the secondary depending on the desired output signal and on how much ringing due to parasitic capacitances in the coil can be tolerated.

The sensitivity is about 5 to 10 μV rms of second harmonic per gamma, depending on the excitation frequency and the number of secondary turns.

The output signal from the unloaded sensor contains a large amount of fundamental and higher odd harmonics of the excitation voltage. Some of this is due to an unavoidable nonorthogonality between the excitation and secondary winding (residual transformer action) and some is due to twisting stress or to other factors introducing magnetic anisotropy.

With the excitation adjusted to give near-maximum second harmonic output (about 260mA rms excitation current with 12 turns) three fluxgates gave 12 to 18 μV, 20 to 26 μV and 10 to 15 μV rms minimum second harmonic with excitation frequency 1250Hz and 2000 turns on the secondary winding, corresponding to 1-3γ equivalent residual signal. Table 1 gives a frequency analysis of the sensor output at null.

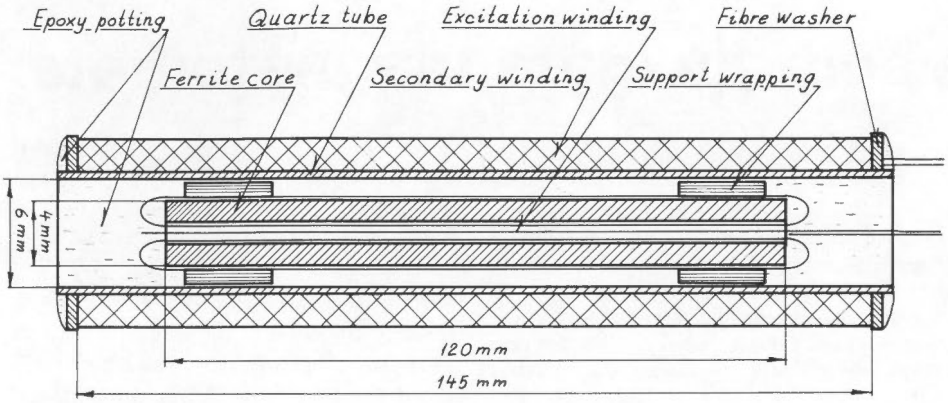

Figure 1. Sensor.

Loading the sensor output with a capacitor shows the well known parametric amplification (Serson and Hannaford, 1956), and a resistive load attenuates the higher frequencies as in an LR low-pass filter. These measurements were made with less than −80 dB second harmonic content in the excitation current.

The effect of injecting second harmonic in the excitation has been investigated by measuring the shift in minimum second harmonic feed-through when the phase of the injected second harmonic is shifted (Table 2).

We see that .1 per cent second harmonic increases the second harmonic feed-through by 10 to 20 dB.

The variation is due to the degree of cancelling or enhancement between the original and the injected second harmonic. These results indicate that when .1 per cent (−60 dB) second harmonic in the excitation has a measurable effect, the second harmonic content in the excitation should be suppressed below .01 per cent (−80 DB).

Block diagram and design principles

A block diagram of the magnetometer is shown in Figure 2.

A very low distortion, amplitude-stabilized Wien bridge oscillator, and a tuned power amplifier provide the 260 mA rms excitation current. The second harmonic content in the excitation current is below −80 dB and the 10μF coupling and tuning capacitor blocks any DC current in the excitation circuit. A reversal switch to check excitation symmetry is provided together with a voltage drop resistor of 1Ω to monitor the excitation current.

The fluxgate output signal is amplified through a Twin-Tee amplifier and fed to the phase detector bridge. The reference voltage for the phase detector bridge is generated by phase-locking to the excitation signal a VCO multivibrator, running at the second harmonic.

The phase-lock reference generator is very easily phase adjustable and has very little phase shift with changes in temperature and frequency. It is certainly much less than the phase shift of a double rectifier plus tuned amplifier system, if the same low content of odd harmonics is desired.

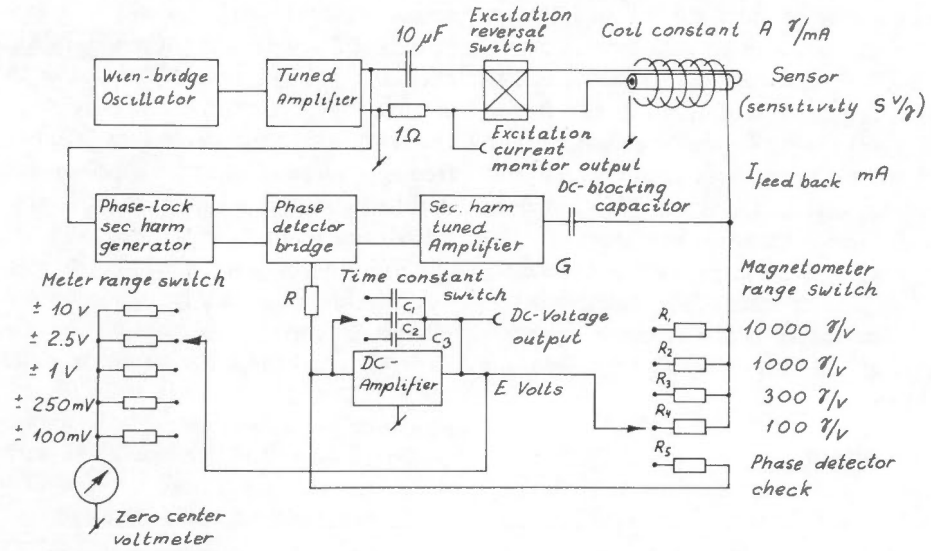

Figure 2. Block diagram of magnetometer.

Table 1
Frequency Analysis of Fluxgate Output

Total output signal (unloaded)	220 mV p-p (rms)
Fundamental (1236Hz)	15.5 mV
Second harmonic	19 μV
Third	8.3 mV
Fourth	34 μV
Fifth	7.8 mV
Sixth	50 μV
Seventh	7.6 mV
Eighth	2.5 μV
Ninth	6.0 mV
Tenth	not measurable (<1μV)

Table 2
Effect of Second Harmonic in Excitation

Injected Second Harmonic	Phase	Mininum Second Harmonic Output (arbitrary level)
(%)	(°)	(dB)
0	–	<−100
1	0	−90
	180	−80
1	0	−71
	90	−64
	180	−78
10	0	−51
	90	−43
	135	−53
	100	−45

The only phase shift that could affect the operation of the phase detector is thus the phase shift in the sensor due to

hysteresis (see Coleman, 1959) and the phase shift in the second harmonic tuned amplifier.

To reduce the temperature changes in phase shift the sensor secondary is untuned and the amplifier Q is kept as low as possible.

The detector output is fed to an active low-pass filter (integrator) with a DC amplification equal to the open loop amplification of the μA741 operational amplifier in the filter.

The time-constant switch makes it possible to choose between several roll-off frequencies from about .1Hz to 10Hz and the feedback resistor switch selects the magnetometer sensitivity. A centre-zero voltmeter with appropriate ranges is provided for monitoring the output. The last position of the magnetometer sensitivity switch opens the dynamic feedback loop and couples the integrator as a gain 1 amplifier to allow adjustment of the phase alignment of the system.

Effects of phase shift

The output of the phase detector is an AC voltage superposed on a DC level. The DC level is equal to the rms value of the input signal multiplied by the cosine of the phase angle ϕ between the reference and the input signals.

From Figure 3 the following equations are derived for the dynamic performance of the feedback system:

$$\Delta H = \left(H - e_2 \cdot \frac{A}{R_f} \right)$$

$$G_3 = \cos\phi$$

where ϕ is the phase angle between reference and input signals.

$$e_2 = \Delta H \cdot G_1 \cdot G_2 \cdot G_3 \left(\frac{1}{j\omega RC + \frac{1}{G_4}} \right)$$

which gives

$$H = e_2 \cdot \frac{A}{R_f} \cdot \left(1 + \frac{1 + j\omega RCG_4}{G_1G_2G_3G_4 \frac{A}{R_f}} \right)$$

The steady-state value of H is thus

$$H \overset{\cong}{0} e_2 \cdot \frac{A}{R_f}$$

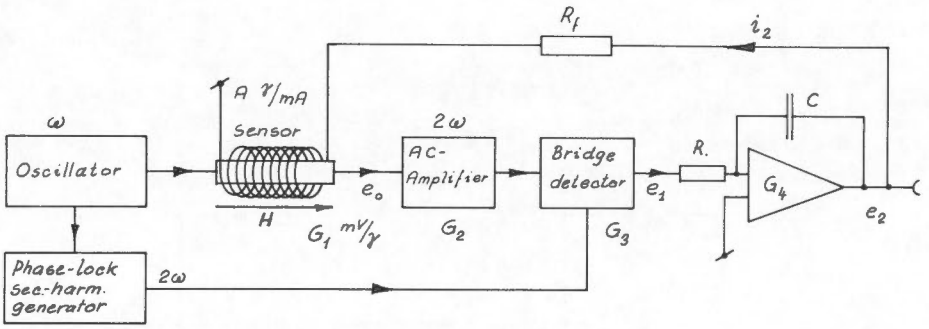

Figure 3. Signal flow diagram of magnetometer.

which gives $\frac{A}{R_f} G_1G_2G_3 = 2 \gg \frac{1}{G_4}$ and $\omega_u = \frac{2}{RC} \simeq 35$ rad/sec $\simeq 5$ Hz

and the frequency response is determined by

$$\frac{H}{H_0} = 1 + \frac{\frac{1}{G_4} + j\omega RC}{G_1G_2G_3 \frac{A}{R_f}} =$$

$$\frac{G_1G_2G_3 \frac{A}{R_f} + \frac{1}{G_4} + j\omega RC}{G_1G_2G_3 \frac{A}{R_f}}$$

This is shown in Figure 4. Typical values of the parameters are

$G_4 = 15{,}000$
$G_1 = 10\,\mu V/\gamma = 1$ V/Oe
$A = 18\,\gamma/\mu A = 180$ Oe/A
$R_f = 18K\Omega$
$G_2 = 200$
$G_3 = \cos\phi = 1$ (for proper phase alignment)
$R = 27K\Omega$
$C = 2\mu F$

The time constant is

$$\tau = \frac{1}{\omega_u} \simeq 0.03 \text{ sec}$$

This system is inherently stable, and the time-constant may be changed by changing any of the parameters except G_4. To keep the same time-constant for different sensitivities we should be able to change C simultaneously with R_f.

For short time-constants, second harmonic ripple on e_2 may be a consideration, especially if the phase-sensitive detector is not well balanced.

If $G_3 = \cos\phi$ changes because of variation in the phase shift of the sensor or the AC amplifier, the first effect is a change in time-constant; secondly the sensitivity changes, as H_0 is not exactly equal to $e_2 A/R_f$ but

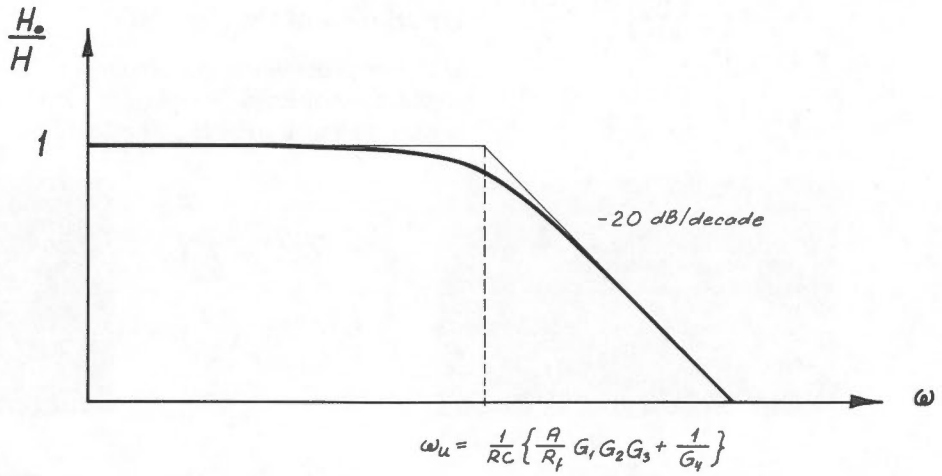

Figure 4. Magnetometer frequency response.

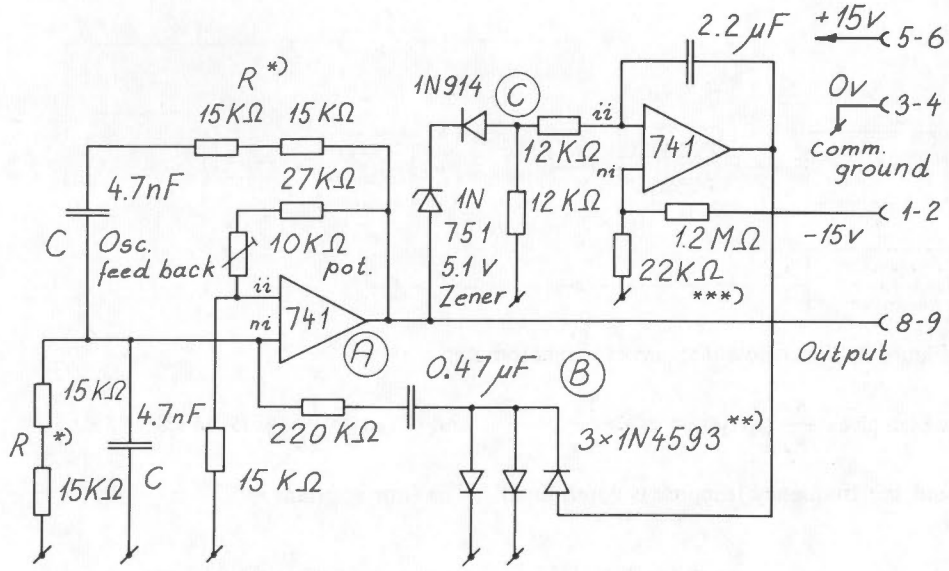

Figure 5. Wien-bridge oscillator.

***The series combination of 4.7nF and two 15kΩ resistors sets the oscillator frequency at 1154Hz and by using 4.7nF and 15kΩ to build a T-T network a second harmonic filter is easily made. **The diodes are selected to give lowest second harmonic content in the output. Here the combination shown has proved to be best; but other oscillators may need a different combination. ***Selected to give zero output for zero input of the DC integrator.**

$$H_0 = e_2 \frac{A}{R_f}\left(1 + \frac{1}{G_1G_2G_3G_4 \frac{A}{R_f}}\right)$$

With a large loop amplification $L = G_1G_2G_3G_4A/R_f$ this change is very small, but if an accuracy of $\epsilon = 2 \cdot 10^{-5}$ is wanted, as is the case when the entire z-field is balanced by dynamic feedback, then the allowable change in $G_3 = \cos\phi$ is limited to

$$1 + \frac{1}{L\cos\phi} \leq \left(1 + \frac{1}{L}\right)\left(1 + \epsilon\right)$$

or

$$\cos\phi \geqslant \frac{1}{1 + \epsilon \cdot L}$$

This shows that the loop amplification must be at least 50,000 to give a phase margin of ±60°.

A more indirect source of error due to phase shift variations in the sensor or in the AC amplifier is that the in-phase component of overcoupled second harmonic from the excitation may vary as the over-all phase varies. This will be detected as a drift in the zero offset. One way to avoid this is to keep the second harmonic content in the excitation low.

Description of the electronics

Wien bridge oscillator. The oscillator is an amplitude stabilized Wien-bridge circuit (Figure 5) which has extremely low content of even harmonics. The components in the positive feedback path are high-stability types to minimize frequency drift. The reason for using a series combination of two 15kΩ resistors is to facilitate the later construction of a second harmonic filter (see appendix), which can then be easily made up of the same 15kΩ and 4.7nF components.

The oscillator frequency is $\omega = 1/RC$ and the voltage at the noninverting input of the first μA741 operational amplifier is one third of the output voltage.

The voltage divider from the output to the inverting input is also adjusted to one third, so the common-mode voltage swing of the amplifier inputs is a third of the output voltage. Very delicate regulation of the positive feedback is necessary to keep the amplitude constant and the distortion low. This is accomplished by switching on and off an additional load of 220kΩ on the R-C parallel combination. The switching takes place every time the common-mode voltage is above the forward conduction voltage of the diode parallel-combination. A voltage offset at the noninverting input would bias the diodes asymmetrically introducing even harmonics in the output voltage; but a DC-separation capacitor of 0.47 μF in series with the 220kΩ intermittent load avoids this. The amplitude stabilization takes place by changing the DC bias of the diodes according to a comparison between a zener voltage and the output maximum voltage. Normally this bias is close to zero volts.

Figure 6 shows the output voltage at point *A* and the diode switch voltage at point *B*.

Figure 7 shows the output voltage and the difference voltage between the

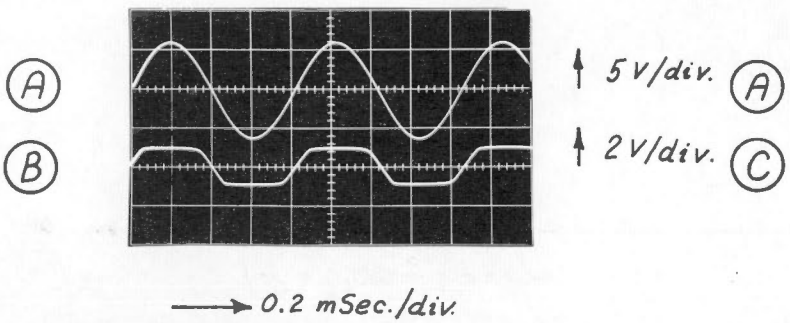

Figure 6. Output voltage and diode switch voltage.

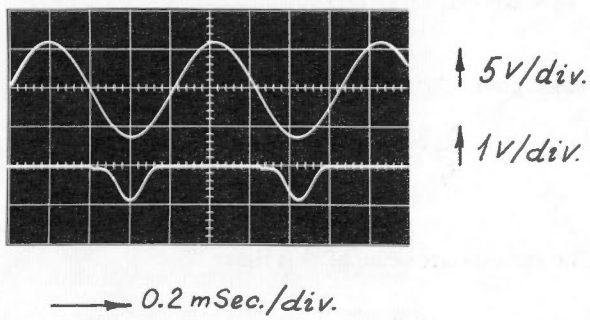

Figure 7. Output voltage and AC regulation voltage.

zener level and the output taken at point *C*.

The content of even harmonics depends on the matching of the stabilizing diodes; oscillators with less than −100 dB second harmonic have been constructed, but normally −80 dB to −85 dB may be expected. Without the DC-separation capacitor, levels of −78 dB to −56 dB second harmonic have been measured.

Excitation amplifier. The excitation amplifier is shown in Figure 8. It is an operational amplifier plus power booster in a gain 1 feedback loop. The output transistors can dissipate 25W and are mounted on a heat sink.

To reduce the collector power the separate power supply for the excitation amplifier is set to ±9V, and a limiting resistor of 5Ω is put in series with the excitation winding.

It was discovered that one source of second harmonic in the excitation was the DC output offset of the amplifier. A DC current in the excitation circuit will displace the operating point of the core B-H loop from the symmetry point and introduce second harmonic. This explains the common experience with DC-coupled circuits that although the output of the amplifier shows very little second harmonic the voltage across the excitation winding may contain a large amount generated in the core.

Because transformers are magnetic devices and thus introduce additional distortion because of asymmetry or overdrive they have been avoided in this circuit, and as offset adjustment of the operational amplifier could not be trusted, we chose to block the DC by two 5μF Mylar capacitors. This reduces the second harmonic and makes it independent of the amplifier offset.

The amplifier is tuned by a Twin-Tee filter designed to give 20 dB (X10) attenuation at the second harmonic. The reason for tuning is not only to reduce second harmonic, but also to reduce the risk of having spurious signals fed through the sensor via a broad-band amplifier.

The 10μF series capacitor tunes the average self-induction of the excitation

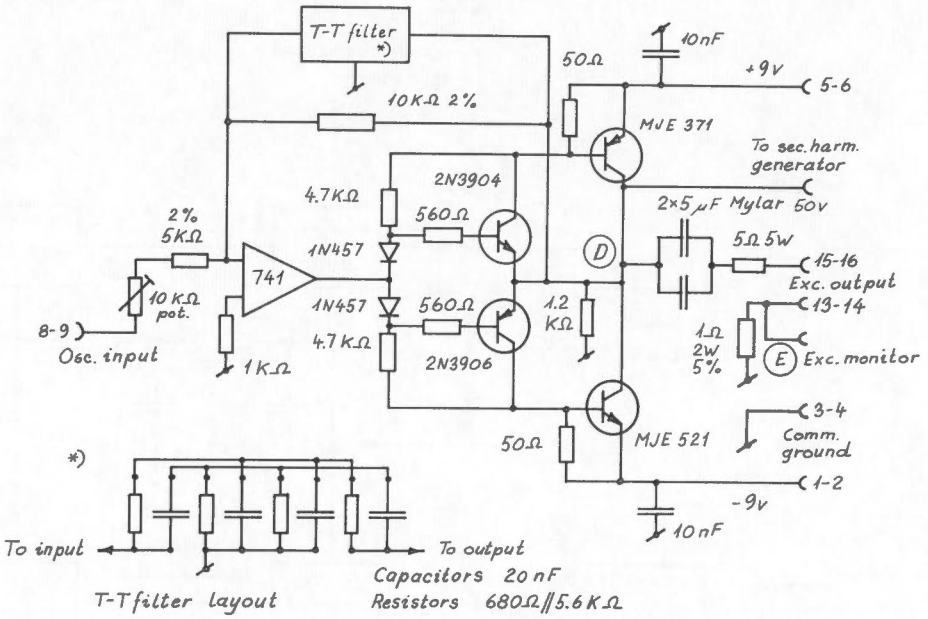

Figure 8. Excitation amplifier.

winding to resonance, so that the current and the voltage delivered by the amplifier are in phase as shown in Figure 9; since the damping from the series resistors is rather heavy parametric resonance amplification in the excitation circuit as described by Ling (1963) does not take place.

If low power consumption of the excitation amplifier is essential this parametric resonance may be established by reducing the series resistor to 0.1Ω (for monitoring the excitation current) and increasing the capacitor to about 40μF (for 1250Hz excitation). The current peaks in Figure 9 then become very narrow and high so a very high maximum current can be obtained for a low rms value.

Table 3 gives the data for parametric resonance at 1250Hz; the rms current is measured with an AC amperemeter, E_{drive} is the amplifier output voltage, and E_{ex} is the voltage across the excitation winding.

Table 3
Parametric Resonance of Excitation Circuit

f	1250Hz
E_{drive}	6V p-p
C	45μF
I	400 mA rms
E_{ex}	12V p-p
I_{ex}	8A p-p

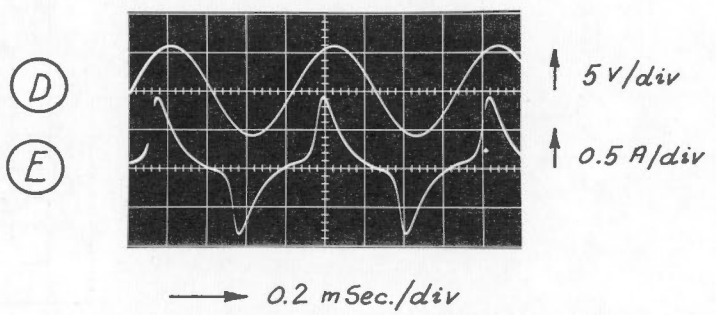

Figure 9. Output voltage and current of excitation amplifier.

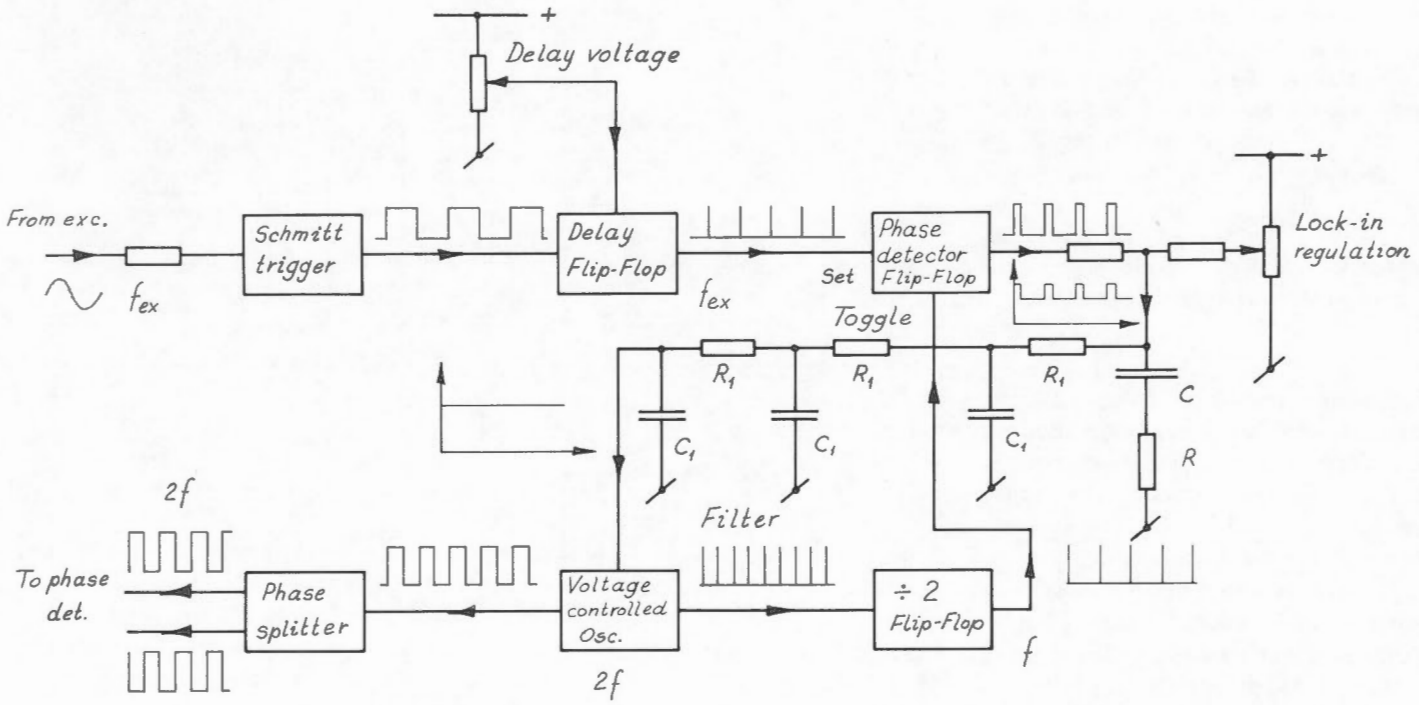

Figure 10. Block diagram of phase-lock system.

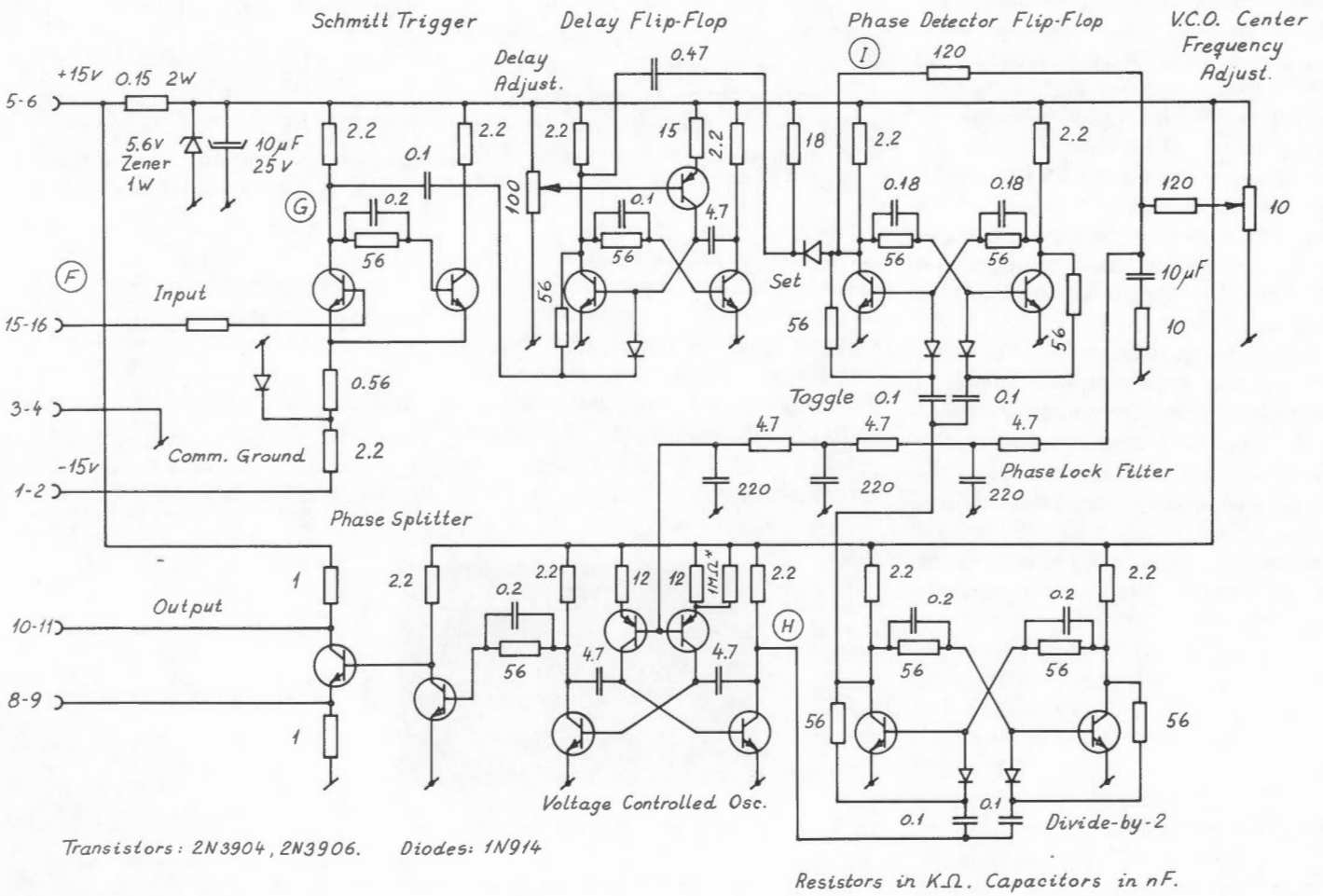

Figure 11. Phase-lock second harmonic generator.

In the normal excitation mode shown in Figure 9 and used in this instrument the typical data are as seen in Table 4.

Table 4
Frequency Analysis of
Excitation Current

f	1154Hz
I_{ex}	1.8 A p-p
I	300mA rms
	(dB)
Second harmonic	< −80
Third	− 8
Fourth	<<−80
Fifth	−15

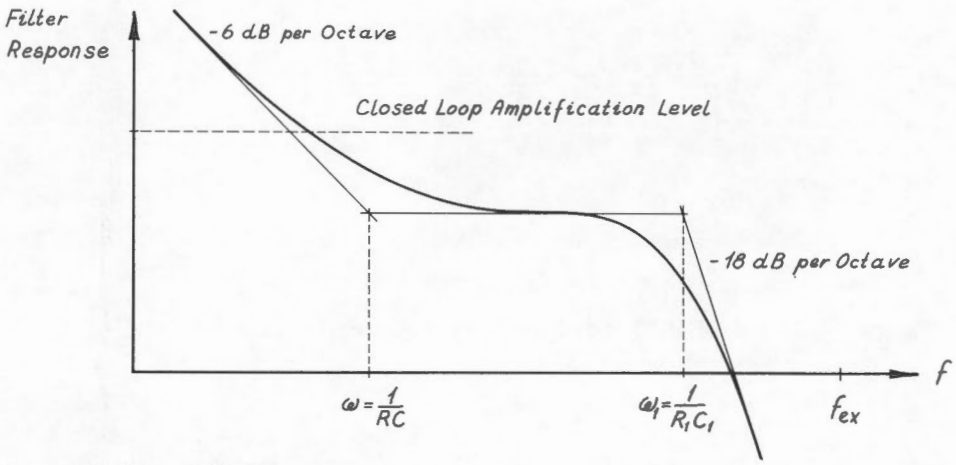

Figure 12. Phase-lock filter response.

Phase-lock second harmonic generator. A block diagram is shown in Figure 10 and a detailed circuit diagram in Figure 11.

The dynamic performance of the phase-lock system, such as the lock-in range and the transient response is determined by the loop gain and the filter characteristic. The phase-detector output contains square-wave pulses of frequency f_{ex} and a sawtooth wave of frequency $(f_{ex}-f) = f_s$. To avoid any trace of f_{ex} and its odd harmonics in the $2f$ output of the VCO the filter must attenuate the frequency f_{ex} to a negligible amount. At the same time the filter must allow enough signal at the frequency f_s to pass so that the system will be able to lock in if the free-running VCO frequency is different from $2f_{ex}$ by this amount. Being a feedback system, the open-loop frequency response must show a safe −6 dB/octave roll-off down to the closed loop amplification point as in normal feedback amplifiers; below this point the characteristic may be horizontal again and then roll off as rapidly as wanted just before f_{ex}. This is done with a filter whose characteristic is shown in Figure 12.

The system combines a wide lock-in range with an adequate rejection of f_{ex}. The amount of f_{ex} in the VCO output is −79 dB and $3f_{ex}$ is −80 dB down.

The lock-in potentiometer is adjusted to give a symmetrical output waveform from the phase detector to ensure that f_{ex} is close to the centre of the lock-in range of the system. Figure 13 shows the excitation voltage taken at point F and the Schmitt-trigger output at G. Figures 14, 15 and 16 show the VCO output at H and the phase detector output at point I for three positions of the lock-in potentiometer.

AC amplifier. The first stage of the AC amplifier shown in Figure 17 is a Twin-Tee active filter designed to give a gain of 100 at $2f_{ex}$ and an attenuation of 20 dB relative to this at f_{ex} and $3f_{ex}$. The two following stages are a gain 5 amplifier and a gain 1 inverter.

The necessary AC amplification is determined by the zero drift vs. temperature and time of the output DC amplifier. A conservative estimate of this is 1 to 3mV, i.e., of the same order of magnitude as the zero offset of the amplifier. Since the sensor output is 5 to 10μV rms per gamma an AC amplification of about 500 is necessary to make the DC offset drift correspond to less than 1γ.

The content of fundamental and third harmonic in the fluxgate signal is about 20mV rms and 10mV rms, respectively. To avoid saturation of the phase detector only about 50 times amplification of these frequencies can be tolerated, giving 3V p-p fundamental and 1.5V p-p third harmonic.

Figure 18 shows the input signal taken at K and the filtered output at L.

Because the fluxgate signal at K is damped by the input resistor of 4.7kΩ ringing between the secondary winding and cable and parasitic capacitances is avoided. The second harmonic is attenuated only 1 or 2 dB and the phase shift is negligible.

The AC amplifier output shows 60Hz modulation of the second harmonic from the 60Hz field present everywhere in the laboratory. The signals are photographed with the magnetometer feedback loop closed so it represents the null output from the sensor. A frequency analysis of the two signals is given in Tables 5 and 6.

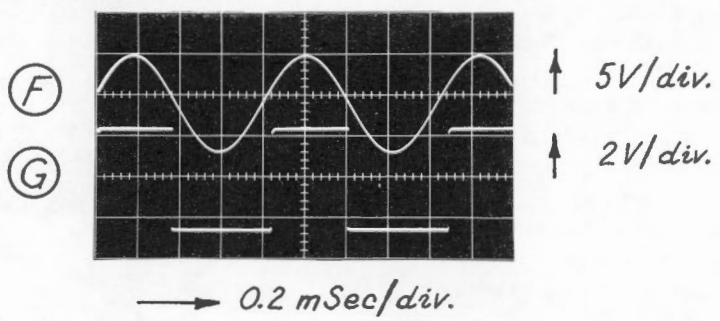

Figure 13. Excitation voltage and Schmitt trigger output.

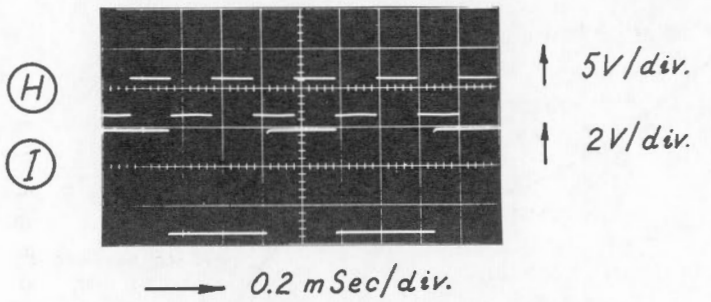

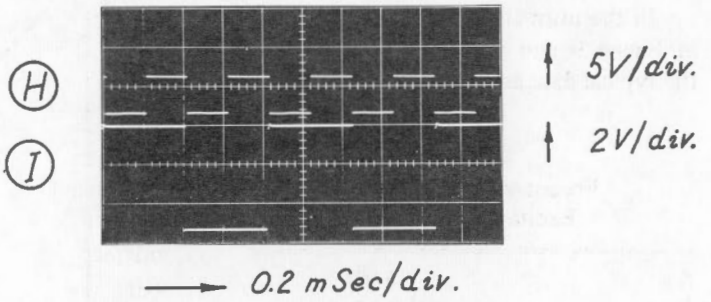

Figures 14, 15 and 16. VCO and phase detector outputs.

Table 5
Frequency Analysis of
Fluxgate Null-output

(Hz)		(rms)	
	Dynamic feedback		
1154	fundamental	19mV	
2308	second harmonic	35μV	± 60Hz sidebands
3462	third harmonic	10mV	

Table 6
Frequency Analysis of AC
Amplifier Output

(Hz)		(rms)	
	Dynamic feedback		
1154	fundamental	1.1V	
2308	second harmonic	25mV	± 60Hz sidebands
3462	third harmonic	.62V	

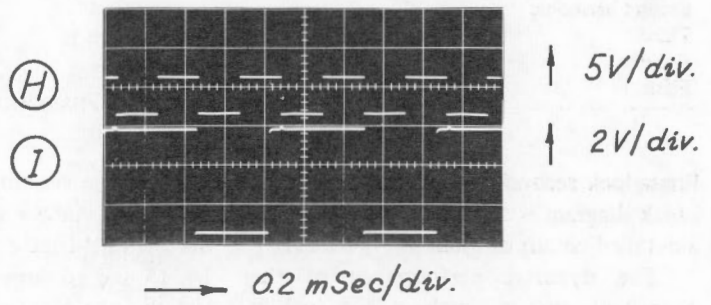

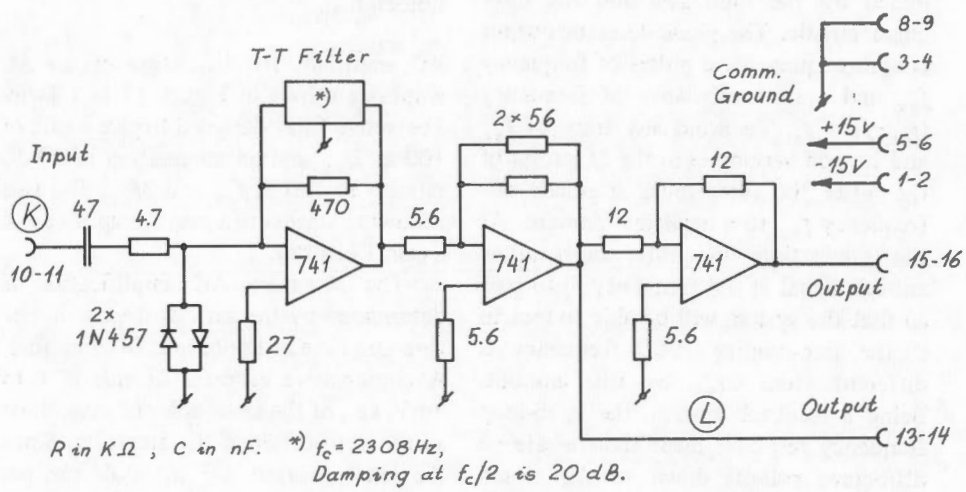

Figure 17. AC amplifier.

Detector and DC amplifier. The phase detector is of the diode bridge type which is free from any internal zero offset or drift (Figure 19).

The reference and the input signals are DC-separated from the bridge by coupling capacitors and the zero levels of the two signals are defined by voltage dividers. Two antiphase AC signals are fed to the bridge and depending on the reference signal polarity one or the other of the input signal levels is transferred to the output of the bridge.

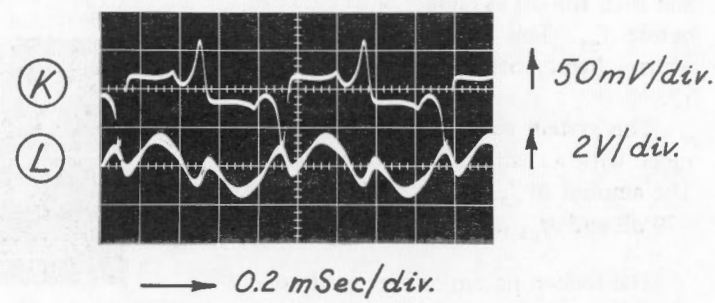

Figure 18. Damped fluxgate null signal and AC amplifier output.

Figure 20 shows the AC input signal at *M* and the detector output signal at *N*. Normally the potential at *N* is zero but to show the detector output signal the connection to the output amplifier has been removed. This opens the dynamic feedback loop so that the signal contains more second harmonic than shown in Figure 18. Figure 20 shows that the AC signal is chopped and inverted twice for every period of the reference. This makes the detector sensitive to any second and higher even harmonic in the AC signal but insensitive to fundamental and odd harmonics. A 4V p-p fundamental at the AC inputs affects the DC level of the detector output less than 1γ equivalent. The DC amplifier integrates the detector output removing any reference or AC signal.

The secondary winding of the fluxgate sensor has a coil constant of about 18γ/μA and the DC amplifier is capable of delivering ±10V output. To balance out ±100,000γ a series resistor of 1.8kΩ is needed, using about 5.5mA.

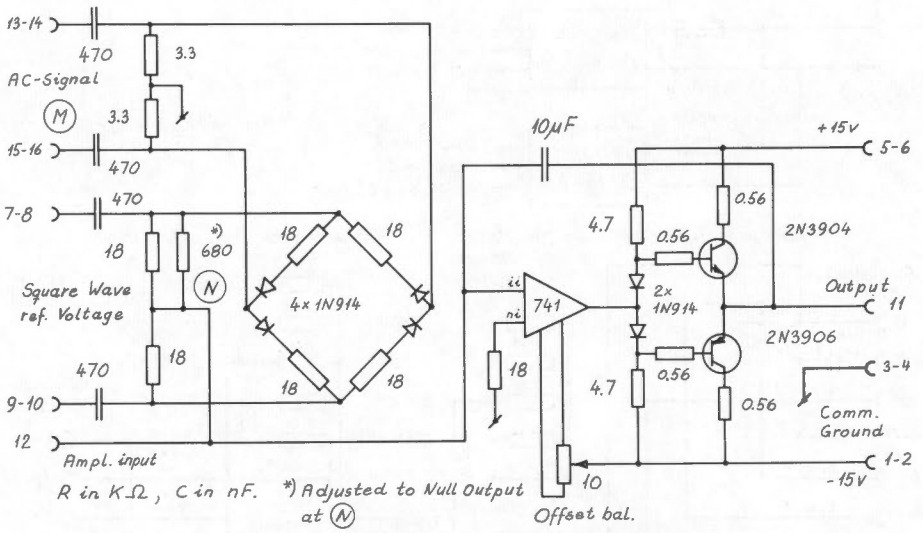

Figure 19. Detector and DC amplifier.

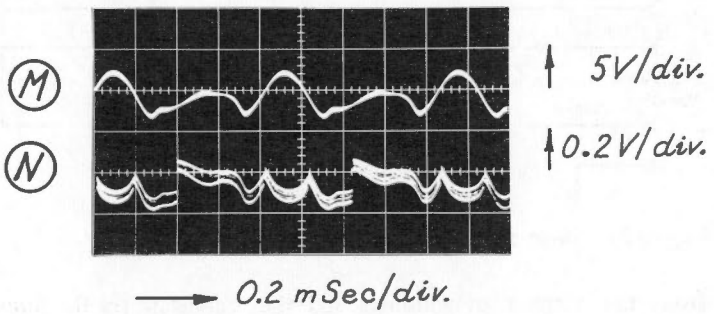

Figure 20. Phase detector bridge input and output signals.

Figure 21. Interconnections between card plugs.

Interconnections between card plugs. The interconnections between the card plugs are shown in Figure 21.

Front panel connections and power supply. The front panel connections and power supply are shown in Figure 22.

Performance tests

Time-constants. To measure the time-constants a square-wave field was applied to the sensor by connecting a square-wave voltage to the secondary coil via a large series resistor. Figure 23 shows the response of the magnetometer output with the short time-constant and Figure 24 shows the response with the long time-constant. The upper traces are the square-wave voltages supplied to the secondary coil via a 10MΩ resistor and the lower traces show the magnetometer response.

The coil constants for the secondary coils of three fluxgates are calculated

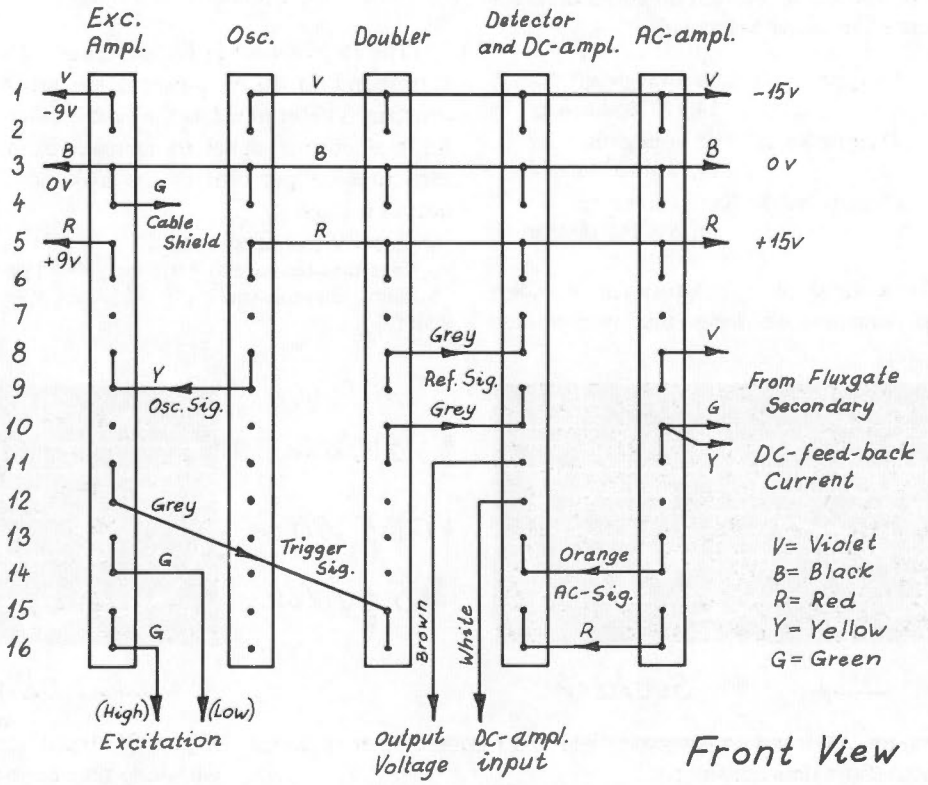

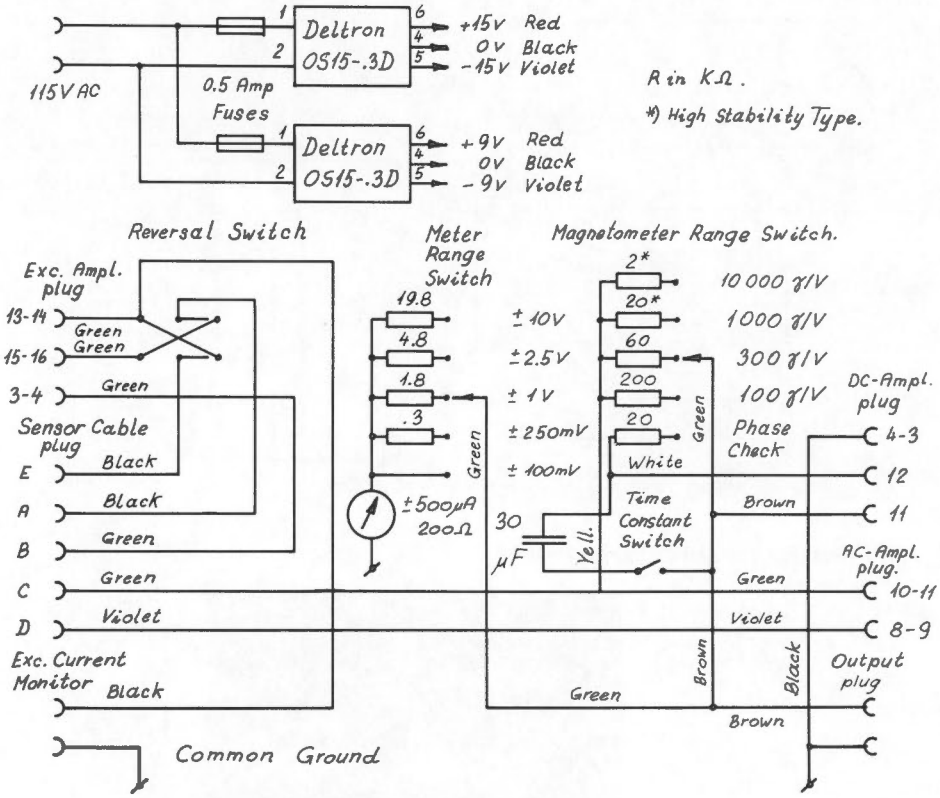

Figure 22. Power supply and front panel connections.

from the number of windings and the winding length. As the diameter is 6mm and the length 14.5cm no corrections for end effects have been made.

Fluxgate No. 1: 2028 turns giving 14.0×10^3 turns/m

Fluxgate No. 2: 2048 turns giving 14.13×10^3 turns/m

Fluxgate No. 3: 2060 turns giving 14.25×10^3 turns/m

As a field of 1 mA-turns/m = $0.4\pi\gamma$ in vacuum we have the average coil constant for the three coils:

$$A = 14.13 \times 0.4\pi = 17.8\gamma/\mu A$$

The steps shown in Figures 23 and 24 correspond to 10.7γ p-p, and the time-constant is determined as the time it takes for the output signal to increase from zero to 63.3 per cent of the maximum output voltage.

From the figures we find:

Long time-constant $\tau_1 \simeq 1.5$ sec; $f_1 \simeq 0.1$Hz

Short time-constant $\tau_2 \simeq 0.32$ sec; $f_2 \simeq 0.5$Hz

Output signal noise. Figure 25 shows a 50-second recording of the magnetometer output. One vertical division corresponds to 0.5γ; the time-constant is $\tau_1 = 1.5$ seconds or upper frequency $f_1 = 0.1$Hz. Superposed on the 1.8γ p-p micropulsation is a noise level of 0.1 – 0.3γ p-p.

Sensor zero offset. The zero offset is determined as half the difference between two measurements of $\overline{F}$, one with the sensor pointing downwards and one upwards. The magnetometer output voltage is measured with a 5-digit digital voltmeter and the magnetometer sensitivity is set to 10,000 γ/V giving about 6.0000 volts to compensate $\overline{F}$; the last digit then corresponds to about 1γ.

The following tests showed that the observed offset could not be attributed to the electronics. Reversal of the excitation current had no effect on the voltmeter reading which means it is less than 0.5γ. The phase detector could be adjusted about ±45° from the proper phase alignment with less than 2γ change in voltmeter reading, and a ±1mV DC offset adjustment of the DC amplifier had no effect on the output. Reversal of the voltmeter connections similarly showed no change in the reading apart from change of sign. Switching off and on of the excitation current changed the reading by 0 - 1γ and a 360° rotation of the sensor also gave readings within 1γ. The phase detector showed a DC shift of less than 1γ equivalent for a 4V p-p fundamental voltage input, and the actual total input voltage as shown in Figure 18 is less than 2V p-p.

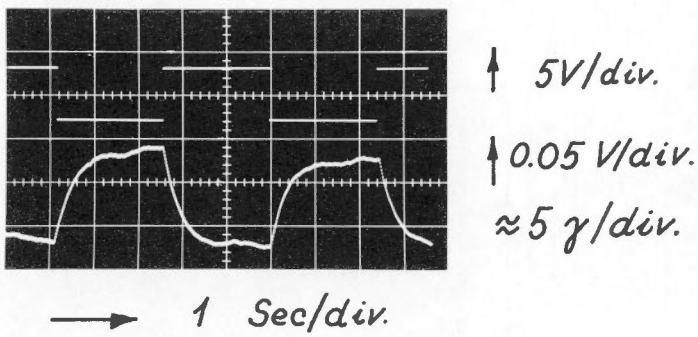

Figure 23. Input square-wave field and magnetometer response with short time-constant.

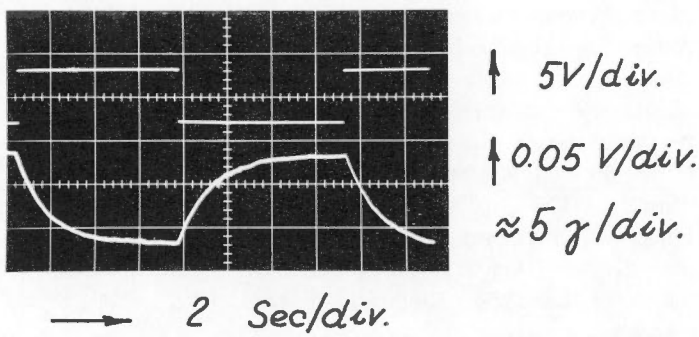

Figure 24. Input square-wave field and magnetometer response with long time-constant.

Sensor No. 1 showed a large offset of +100γ*
Sensor No. 2 showed −4γ to −8γ offset
Sensor No. 3 showed −2γ offset

For comparison, one of the Dominion Observatory mu-metal fluxgates was measured and an offset of −20γ to −25γ was found.

The source of this offset is normally attributed to residual permanent magnetization of the sensor core. However it is difficult to see how a core could maintain any permanent magnetization when it is deeply saturated twice every excitation cycle.

For fluxgate sensor no. 2 the offset variation vs. time has been investigated for 10 days (Table 7).

Table 7

Fluxgate Offset Variation

Date	Measurements	Offset
(1969)	(volts)	(γ)
24 Oct.	− 6.7265	
	+6.7249	−7
28	+6.7244	
	− 6.7261	−7
29	− 6.7271	
	+6.7255	−7
31	+6.7259	
	− 6.7275	−7
4 Nov.	+6.7236	
	− 6.7251	−7
4	+6.7257	
	− 6.7267	−4
5	+6.7236	
	− 6.7248	−5

Magnetometer constant $0.87 \times 10^{+4}$ γ/V.

*This sensor was later demagnetized in the AC demagnetizing coil belonging to the paleomagnetic group at the Dominion Observatory. The first attempt was made with ±100 oersted maximum AC field but this did not remove the offset. Then the maximum obtainable field ±3000 oersted was used and this reduced the offset to less than 2γ. The ferrite material apparently contains a few very sticky domains which the excitation field is completely inadequate to wipe out.

These readings have all been taken with I_{exc} = 260mA rms. Temperature tests have been carried out between the two offset determinations on November 4, 1969; during these tests null field was established by means of a set of three orthogonal Helmholtz coils (Roy, *et al.*, 1969) and the sensor then showed −5γ offset independent of the sensor attitude.

If the excitation current exceeds a certain magnitude (300mA rms in this case) the offset increases. This is clearly

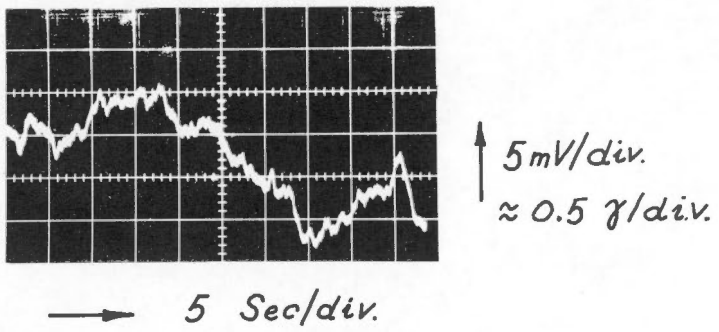

Figure 25. Magnetometer output noise.

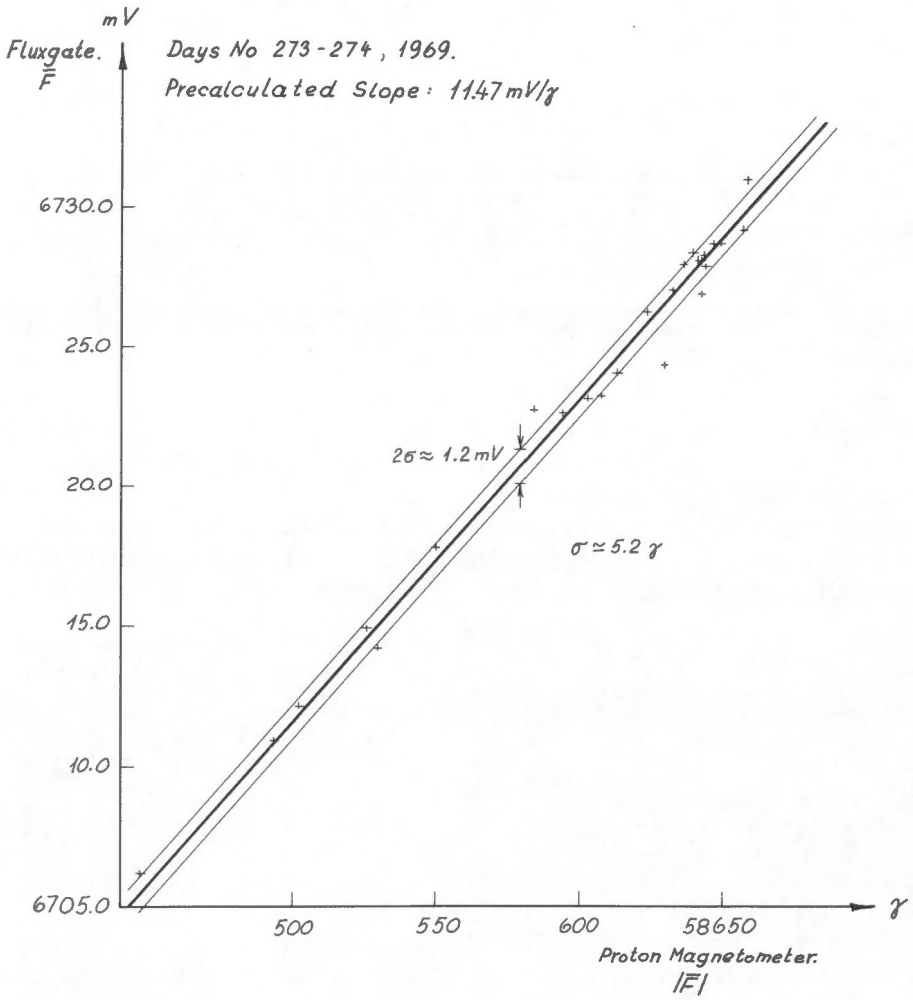

Figure 26. Comparison between fluxgate and proton magnetometer for day 273-274, 1969.

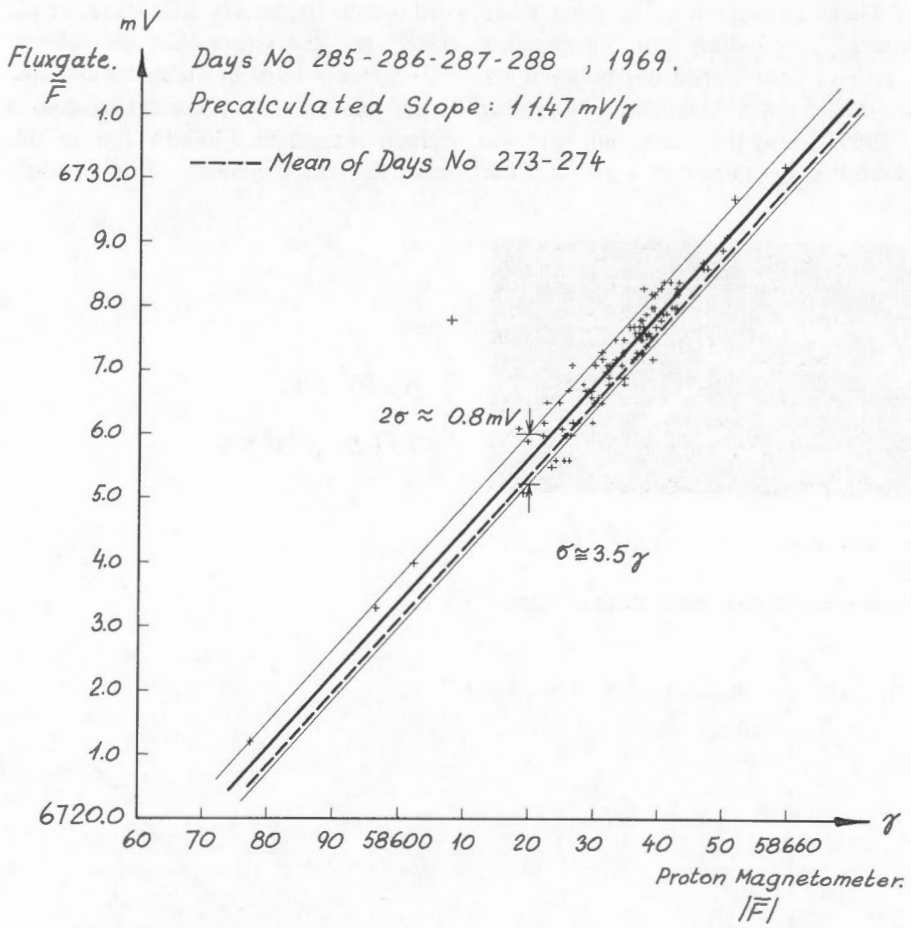

Figure 27. Comparison between fluxgate and proton magnetometer for days 285-286-287-288, 1969.

due to second harmonic in the excitation as an excitation reversal showed 5γ shift at 305mA and 27γ shift at 325mA; below 300mA the shift was less than 1γ for excitation reversal. Varying the excitation current between 170mA rms and 300mA rms showed 1γ or less shift in output reading compared to 230mA rms.

Stability test. A 15-day preliminary stability and drift test was performed from September 30 (day no. 273) to October 15, 1969 (day no. 288). The fluxgate sensor was mounted on a theodolite and positioned parallel to the earth's field by adjusting to maximum reading. In this position the sensor will measure the total field $\bar{F}$ with an error less than 1γ if the sensor attitude is stable within ± 1/3° or if the field component perpendicular to the mean $\bar{F}$ direction is less than ±340γ. This setup allows a very convenient comparison with a proton magnetometer as long as the field is not too disturbed. The room was controlled by thermostat to within 2 or 3°C.

The means of the proton magnetometer and fluxgate readings for the first 10 minutes of every full hour were plotted against each other, and the mean was determined by fitting a line with precalculated slope to the points. The slope is taken as the ratio between the fluxgate and the proton magnetometer readings for a point near the middle of the cluster.

As an estimate of the standard deviation σ two lines were fitted parallel to the mean line so they would enclose between them 63 per cent of the points. σ is then taken at half the vertical distance between these 63 per cent limiting lines.

The proton magnetometer readings were taken from an AMOS automatic observatory (Andersen, 1969); the printout of the tape included 10-minute mean values given with an accuracy of 0.1γ. The fluxgate output was digitized by a HP 3460B digital voltmeter where the last digit represented approximately 1γ. The last three digits were converted to an

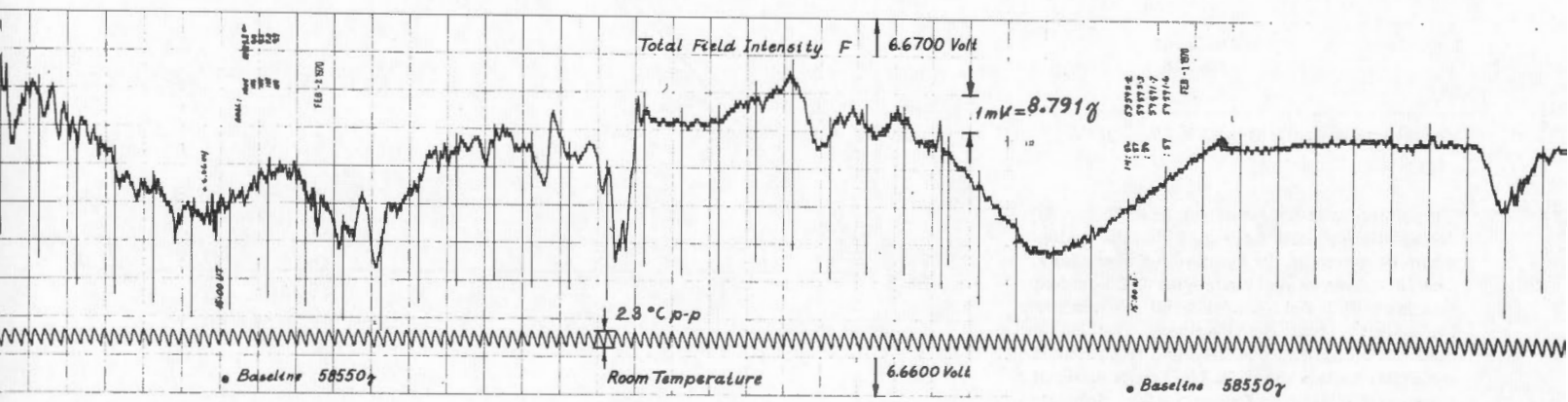

Figure 28. Fluxgate record.

analog signal and recorded by a Moseley potentiometer recorder. With full-scale deflection of 1000γ the uncertainty of the recorder is estimated to be 2 to 5γ.

The plots for day 273-274 and for days 285-286-287-288, 1969 are shown in Figures 26 and 27.

From the first plot is derived $\sigma \simeq 5.2\gamma$ and for the second, $\sigma \simeq 3.5\gamma$ comparable to the recorder uncertainty. The difference in means of the two plots is 2.5γ over 15 days.

A further stability test begun on December 24, 1969 is still going on (March 1970). The earlier setup has been changed from recording the three last digits to the two last digits of the voltmeter output, giving a full-scale deflection of approximately 100γ and easily recognizable steps of about 1γ on the record. Since January 13, 1970 the baseline has been determined every day at 1500 UT by comparing three to five single proton magnetometer readings with the corresponding fluxgate readings. The average value of the three to five baseline determinations is taken as the baseline value for that day. Figure 28 shows an example of the record and Figure 29 shows the baseline determinations. Before January 13 few baseline determinations had been made, each based on only one comparison; they are included in the plot.

For each of the five days January 14 to 18 the baseline was determined from one reading every full hour to investigate the correlation between the fluxgate and the proton magnetometer (Figure 30).

The standard deviations of the points taken for one day at a time range from 0.3γ to 1.0γ and the scatter is believed to be due to the resolution limit of the digital voltmeter whose smallest step is 0.1mV = 0.8791γ, to the small differences in sampling time between the fluxgate and the proton magnetometer, and to the different sampling periods.

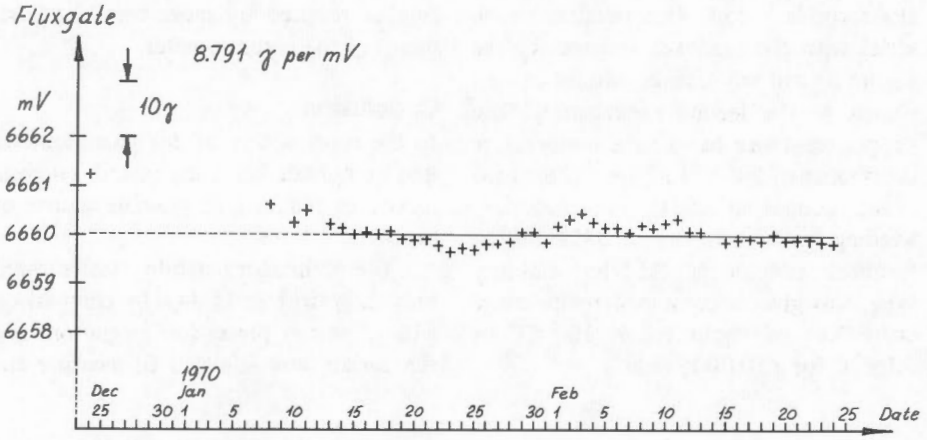

Figure 29. Fluxgate baseline (58550γ), $\bar{F}$.

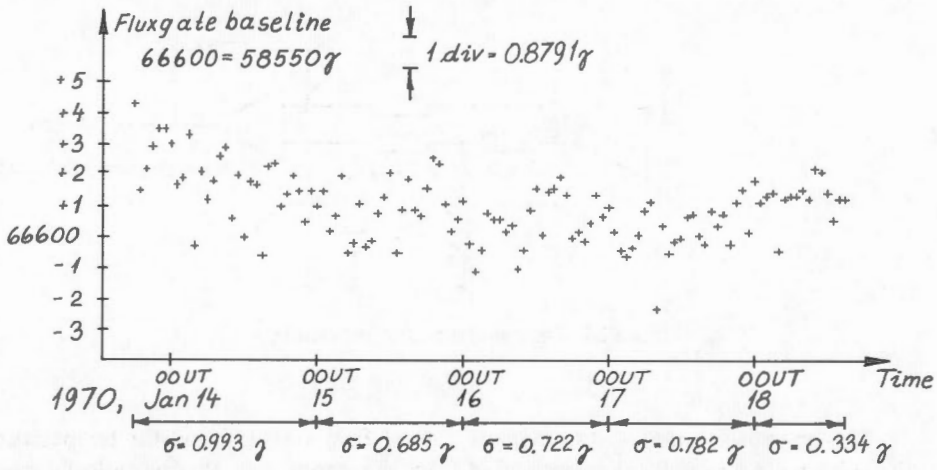

Figure 30. Correlation between fluxgate and proton magnetometer.

Temperature coefficient of sensor. To determine the temperature coefficient, the sensors have been placed inside a nonmagnetic box with thermostatically controlled temperature. With the sensor in position to measure F the following readings have been taken:

Fluxgate No. 2

Reading	Temp.	
−6.7236 V	21°C	
−6.7286 V	39°C	$\alpha_2 = 2.4\gamma/°C$

magnetometer constant $0.87 \times 10^{+4}\gamma/V$

Fluxgate No. 3

Reading	Temp.	
−6.7247 V	19°C	
−6.7315 V	40°C	$\alpha_3 = 2.8\gamma/°C$

With sensor no. 2 in near-zero field established by dynamically balancing the earth's field with a three-axis Helmholtz coil system (Roy, *et al.*, 1969), less than 1γ change for 14°C temperature change was measured.

Reading	Temp.	
−0.0120 V	24.5°C	
−0.0119 V	38.5°C	$\alpha < 0.1\gamma/°C$

The temperature dependence may be due to several factors; one commonly considered is the change in secondary coil constant caused by the length expansion coefficients of the quartz tube or of the copper winding. The fused quartz tube has a temperature expansion coefficient of 0.3 to 0.5×10^{-6}/°C corresponding to 0.02 to 0.03γ/°C and the copper of the secondary winding has 14 to 18 $\times$ 10^{-6}/°C corresponding to 0.8 to 1.1γ/°C.

Another source of temperature dependence may be the inhomogeneity of the bucking field (see Ledley, 1969). If the ferrite core is shifted or expands inside the secondary coil it might over its length see a different field. However, end correction coils of various shapes and sizes have been used on the secondary winding with no success at all.

A third possibility is the temperature dependence of the copper resistance of

the secondary coil. This resistance is in series with the feedback resistor R_f (see Figure 3) and any changes would cause a change in the feedback current i_2. The copper resistance has a large temperature coefficient of 3.8×10^{-3} per °C for hard drawn copper at 20° C. The secondary winding has a resistance of 33Ω and the feedback resistor is 2kΩ high-stability type; this gives a combined temperature coefficient of about 6.2×10^{-5}/°C or 3.1γ/°C for a 50,000γ field.

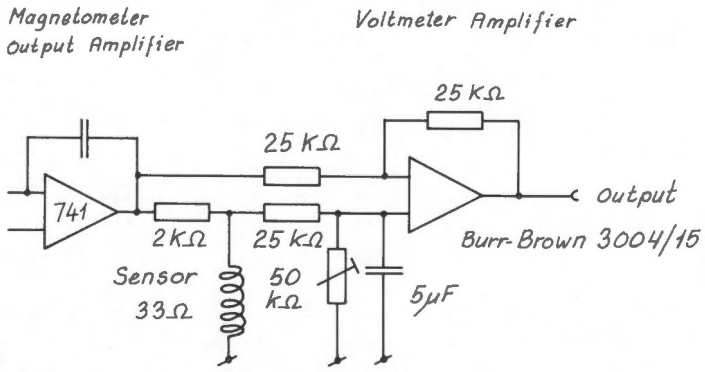

Figure 31. Temperature compensation.

The obvious solution was to measure the voltage drop over R_f alone instead of the voltage over the combined R_f and secondary winding, but surprisingly this gave a negative temperature coefficient of -2.2γ/°C, indicating that the coil constant has this negative coefficient and the copper resistance contributes with about 5γ/°C.

The fact that the DC voltage across the secondary winding varies with temperature gives the possibility of using the copper in this winding as a thermo sensor. The circuit is shown Figure 31 where the differential DC amplifier measures the voltage from the magnetometer output to a point between the top of the secondary coil and ground. By adjusting the 50kΩ potentiometer a position was found where the magnetometer output changed less than 3.5γ for 20° C change in temperature or less than 0.18γ/°C. This may be further reduced by more careful adjustments of the potentiometer.

Conclusion

In the construction of this magnetometer great emphasis has been placed on eliminating or reducing all possible sources of error.

The preliminary stability test showed only 2.5γ drift in 15 days by comparison with a proton precession magnetometer; the sensor was adjusted to measure the total field vector $\overline{F}$ and the temperature in the room was thermostatically controlled to within 2 or 3° C. The sensor showed no temperature coefficient in near-zero field (≅ 120γ) and in 58,600γ the shift was 2.4γ/°C. This temperature dependence has been compensated for by using the resistance of the fluxgate secondary winding as thermo sensor.

A stable zero offset of about 7γ was measured during 10 days; this offset has been attributed to the sensor as attempts to trace it to the electronics have failed.

A second stability test has shown an initial drift of −9γ for the first 20 days followed by random fluctuations of ±3.5γ maximum over the next 60 days. The corresponding standard deviation of the baseline determinations is 1.8γ.

If further tests confirm these findings the fluxgate will have reached the state of development where it is a realistic replacement for the classical magnetometers in geomagnetic observatory instruction.

As the fluxgate performs best when measuring near-zero fields, it is suggested that instead of measuring the usual elements D H Z or X Y Z, it may be advantageous to use a combination of a proton precession magnetometer, measuring F, with two fluxgate sensors, measuring two components perpendicular to each other and to the mean direction of F.

Acknowledgments

This work was carried out under a postdoctorate fellowship granted by the National Research Council of Canada. Thanks for many discussions are given to P.H. Serson, W.L. Hannaford, F. Andersen, and especially to D.F. Trigg, who suggested using a phase-lock system to generate the second harmonic reference voltage.

References

Alldredge, L.R., 1958. Magnetometer, U.S. Patent 2856581.

Andersen, F., 1969. An automatic magnetic observatory (abstract). *IAGA Bull.* 26, 106.

Coleman, Paul J., Jr., 1959. An analysis of the operation of the fluxgate magnetometer. *Space Technology Lab.* Rpt. No. 7320, 2-14.

Joukova, I.S., 1949. About the EMF-spectrum of transverse induction. *Doklady Akademii Nauk SSSR.* 65, 151-154.

Ledley, B.G., 1969. Magnetometers for space measurements over a wide range of field intensities, *Proc. URSI Conf. Weak Magnetic Fields of Interest in Geophysics and Space,* Paris (May).

Ling, S.C., 1963. A fluxgate magnetometer for space applications. *AIAA Summer Meeting,* Paper No. 63-187.

Ling, S.C., 1965. Improved magnetometer uses toroidal gating coil. *NASA,* Technical Brief 65-10103, Goddard Space Flight Center.

Primdahl, F., (in press). The fluxgate mechanism. *IEEE Trans. Magnetics.*

Roy, J.L., W.A. Robertson, and C. Keeping, 1969, Magnetic field-free space for paleomagnetism, rock magnetism, and other studies. *Can. J. Earth Sci.* 6, 1312-1316.

Serson, P.H., and W.L.W. Hannaford, 1956. A portable electrical magnetometer. *Can. J. Technol.* 34, 232-243.

APPENDIX

Twin-Tee active filters

For the symmetrical Twin-Tee filter shown in Figure A1 we have the following definitions:

$$\omega_0 = \frac{1}{RC}, \text{ centre frequency}$$

$$\eta = R_d/2R, \text{ damping ratio}$$

and the relative frequency deviation is

$$\beta = \frac{\frac{\omega}{\omega} - \frac{\omega}{\omega_0}}{\frac{\omega}{\omega_0} + \frac{\omega_0}{\omega}} = \frac{\omega_0^2 - \omega^2}{\omega^2 + \omega_0^2} \simeq -\frac{\omega - \omega_0}{\omega_0} = -\frac{\Delta\omega}{\omega_0}$$

The transfer function is given by

$$\frac{e_i}{e_0} \cdot \frac{R_d}{R_i} = 1 + \eta \cdot \beta + j\frac{\omega}{\omega_0} \cdot \beta \cdot \eta$$

and for $\omega = \omega_0$ is obtained:

$$e_0 = e_i \cdot \frac{R_d}{R_i}, \quad \omega = \omega_0$$

For other frequencies the attenuation relative to this is

$$\Gamma = \left\{(1 + \eta\beta)^2 + \left(\frac{\omega}{\omega_0} \cdot \beta \cdot \eta\right)^2\right\}^{1/2}$$

and the phase shift ϕ is given by

$$\tan\phi = \frac{\frac{\omega}{\omega_0} \cdot \beta \cdot \eta}{1 + \eta \cdot \beta}$$

If the equations are solved for η we get

$$\eta = \frac{-1 \pm \sqrt{\left(1 + \left(\frac{\omega}{\omega_0}\right)^2\right)\Gamma^2 - \left(\frac{\omega}{\omega_0}\right)^2}}{\beta\left(1 + \left(\frac{\omega}{\omega_0}\right)^2\right)}$$

where only the positive solution is possible.

It is then possible to choose the centre frequency ω_0 and the desired attenuation Γ at another frequency ω, and from these calculate the necessary damping ratio η. The filter Q is $Q \cong \eta/\sqrt{3}$.

The Twin-Tee filter of the excitation amplifier is calculated as follows:

Given are: $R_d = 10k\Omega$

for $\omega = \omega_0$: $\frac{e_0}{e_i} = 1$, i.e., $R_i = 10k\Omega$

$$\omega_0 = 2\pi \cdot 1.2 \cdot 10^3 \text{ rad/sec}$$

At the frequency $\omega = 2\omega_0$, 10 times attenuation is wanted: $\Gamma_{2\omega_0} = 10$, and this gives $\eta = 7.1$; $Q \cong 4$.
From this:

$$R = \frac{R_d}{2\eta} = 705\Omega$$

and $$\frac{1}{R\omega_0} = 0.188\mu F$$

As shown in Figure 8 the nearest standard value for the capacitor is chosen and the recalculated resistor value is built up as a parallel combination of two standard resistors. Twin-Tee filters are most conveniently constructed by using four identical resistors and four identical capacitors. Considerable freedom in choice of filter characteristics is obtained by adjusting the filter components to the needs of the amplifier instead of matching the amplifier to a ready-made filter.

As the filter action depends on the degree of rejection of the centre frequency by the Twin-Tee network the component values have to be within 0.5 per cent or better for high-Q filters. For the example given 1 to 5 per cent is adequate as the Twin-Tee network is bypassed by the damping resistor R_d. If the Q is increased the filter will eventually start oscillating.

While the high-frequency response curve continues to roll off, the low-frequency gain goes towards the asymptotic value $2R/R_i$. If this is harmful a capacitor can be put in series with the input resistor giving a high-pass filter with roll-off point at about $\omega_0/2$.

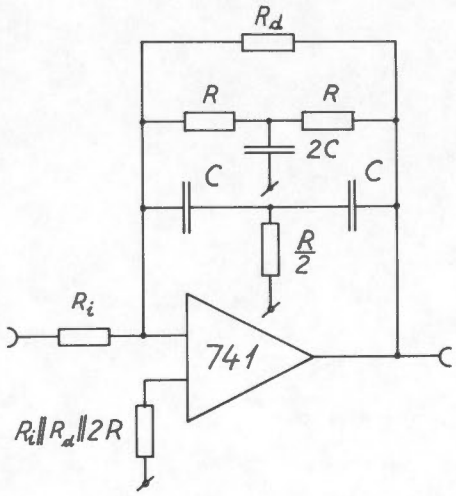

Figure A1. Twin-Tee active filter.